Modeling and Simulation of Molecular Communication Systems With a Reversible Adsorption Receiver

Yansha Deng, *Member, IEEE*, Adam Noel, *Member, IEEE*, Maged Elkashlan, *Member, IEEE*, Arumugam Nallanathan, *Senior Member, IEEE*, and Karen C. Cheung

Abstract—In this paper, we present an analytical model for the diffusive molecular communication (MC) system with a reversible adsorption receiver in a fluid environment. The widely used concentration shift keying is considered for modulation. The time-varying spatial distribution of the information molecules under the reversible adsorption and desorption reaction at the surface of a receiver is analytically characterized. Based on the spatial distribution, we derive the net number of adsorbed information molecules expected in any time duration. We further derive the net number of adsorbed molecules expected at the steady state to demonstrate the equilibrium concentration. Given the net number of adsorbed information molecules, the bit error probability of the proposed MC system is analytically approximated. Importantly, we present a simulation framework for the proposed model that accounts for the diffusion and reversible reaction. Simulation results show the accuracy of our derived expressions, and demonstrate the positive effect of the adsorption rate and the negative effect of the desorption rate on the error probability of reversible adsorption receiver with last transmit bit-1. Moreover, our analytical results simplify to the special cases of a full adsorption receiver and a partial adsorption receiver, both of which do not include desorption.

Index Terms—Molecular communication, reversible adsorption receiver, time varying spatial distribution, error probability.

I. INTRODUCTION

CONVEYING information over a distance has been a problem for decades, and is urgently demanded for multiple distance scales and various environments. The conventional solution is to utilize electrical- or electromagnetic-enabled communication, which is unfortunately inapplicable or inappropriate in very small dimensions or in specific environments, such as in salt water, tunnels, or human bodies. Recent breakthroughs in bio-nano technology have motivated molecular communication [2], [3] to be a biologically-inspired technique for nanonetworks, where devices with functional components on the scale of 1–100 nanometers (i.e., nanomachines) share information over distance via chemical signals in nanometer to micrometer scale environments. These small scale bio-nanomachines are capable of encoding information onto physical molecules, sensing, and decoding the received information molecules, which could enable applications in drug delivery, pollution control, health, and environmental monitoring [4].

Based on the propagation channel, molecular communication (MC) can be classified into one of three categories: 1) Walkway-based MC, where molecules move directionally along molecular rails using carrier substances, such as molecular motors [5]; 2) Flow-based paradigm, where molecules propagate primarily via fluid flow. An example of this kind is the hormonal communication through the bloodstream in the human body [2]; 3) Diffusion-based MC, where molecules propagate via the random motion, namely Brownian motion, caused by collisions with the fluid's molecules. In this case, molecule motion is less predictable, and the propagation is often assumed to follow the laws of a Wiener process. Examples include deoxyribonucleic acid (DNA) signaling among DNA segments [6], calcium signaling among cells [7], and pheromonal communication among animals [8].

Among the aforementioned three MC paradigms, diffusion-based MC is the most simple, general and energy efficient transportation paradigm without the need for external energy or infrastructure. Thus, research has focused on the mathematical modeling and theoretical analysis [9]–[13], reception design [14], receiver modeling [15], and modulation and demodulation techniques [16]–[18], of diffusion-based MC systems.

In diffusion-based MC, the transmit signal is encoded on the physical characteristics of information molecules (such as hormones, pheromones, DNA), which propagate through the fluid medium via diffusion with the help of thermal energy in the environment. The information can be encoded onto the quantity, identity, or released timing of the molecules. In the domain of timing channel, the first work on diffusion based

MC was pioneered by Eckford [9], in which the propagation timing channel is ideally characterized as an additive noise channel. In the domain of concentration-based encoding, the concentration level of information molecules represents different transmit signals. Since the average displacement of an information molecule is directly proportional to the square root of diffusion time [6], long distance transmission requires much longer propagation times. Moreover, the randomness of the arriving time for each molecule makes it difficult for the receiver to distinguish between the signals transmitted in different bit intervals, because the number of received molecules in the current symbol depends on the molecules emitted in previous and current symbols. This is known as intersymbol interference (ISI).

In most existing literature, some assumptions are made in order to focus on the propagation channel. One assumption is that each molecule is removed from the environment when it contributes once to the received signal. As such, the information molecule concentration near the receiver is intentionally changed [19]. Another widely-used idealistic assumption is to consider a passive receiver, which is permeable to the information molecules passing by, and is capable of counting the number molecules inside the receiver volume [14], [20]. The passive receiver model easily encounters high ISI, since the same molecule may unavoidably contribute to the received signal many times in different symbol intervals [21].

In a practical bio-inspired system, the surface of a receiver is covered with selective receptors, which are sensitive to a specific type of information molecule (e.g., specific peptides or calcium ions). The surface of the receiver may adsorb or bind with this specific information molecule [22]. One example is that the influx of calcium towards the center of a receiver (e.g., cell) is induced by the reception of a calcium signal [23], [24].

Despite growing research efforts in MC, the chemical reaction receiver has not been accurately characterized in most of the literature except by Yilmaz *et al.* [15], [16], Tepekule *et al.* [18], and Chou [25]. The primary challenge is accommodating the local reactions in the reaction-diffusion equations. In [15] and [26], the channel impulse response for MC with an absorbing receiver was derived. The MolecUlar CommunicatIoN (MUCIN) simulator was presented in [16] to verify the fully-absorbing receiver. The results in [15] and [16] were then extended to the ISI mitigation problem for the fully-absorbing receiver [18]. In [25], the mean and variance of the receiver output was derived for MC with a reversible reaction receiver based on the reaction-diffusion master equation (RDME). The analysis and simulations were performed using the subvolume-based method, where the transmitter and receiver were cubes, and the exact locations or placement of individual molecules were not captured. They considered the reversible reactions only happens inside the receiver (cube) rather than at the surface of receiver.

Unlike existing work on MC, we consider the *reversible adsorption and desorption* (A&D) receiver, which is capable of *adsorbing* a certain type of information molecule near its surface, and desorbing the information molecules previously adsorbed at its surface. A&D is a widely-observed process for colloids [27], proteins [28], and polymers [29]. Within the

Internet of Bio-NanoThings (IoBNT), biological cells are usually regarded as the substrates of the Bio-NanoThings. These biological cells will be capable of interacting with each other by exchanging information, such as sensed chemical or physical parameters and sets of instructions or commands [30]. Analyzing the performance characteristics of MC systems using biological cells equipped with adsorption and desorption receptors allows for the comparison, classification, optimization and realization of different techniques to realize the IoBNT. The A&D process also simplifies to the special case of an *absorbing* receiver (i.e., with no desorption). For consistency in this paper, we refer to receivers that do not desorb, but have infinite or finite absorption rates, as *fully-adsorbing* and *partially-adsorbing* receivers, respectively.

From a theoretical perspective, researchers have derived the equilibrium concentration of A&D [31], which is insufficient to model the time-varying channel impulse response (and ultimately the communications performance) of an A&D receiver. Furthermore, the simulation design for the A&D process of molecules at the surface of a *planar* receiver was also proposed in [31]. However, the simulation procedure for a *communication* model with a *spherical* A&D receiver in a fluid environment has never been solved and reported. In this model, information molecules are released by the transmission of pulses, propagate via free-diffusion through the channel, and contribute to the received signal via A&D at the receiver surface. The challenges are the complexity in modeling the coupling effect of adsorption and desorption under diffusion, as well as accurately and dynamically tracking the location and the number of diffused molecules, adsorbed molecules and desorbed molecules (which are free to diffuse again).

Despite the aforementioned challenges, we consider in this paper the diffusion-based MC system with a point transmitter and an A&D receiver. The transmitter emits a certain number of information molecules at the start of each symbol interval to represent the transmitted signal. These information molecules can adsorb to or desorb from the surface of the receiver. The number of information molecules adsorbed at the surface of the receiver is counted for information decoding. The goal of this paper is to characterize the communications performance of an A&D. Our major contributions are as follows:

1) We present an analytical model for the diffusion-based MC system with an A&D receiver. We derive the exact expression for the channel impulse response at a spherical A&D receiver in a three dimensional (3D) fluid environment due to one instantaneous release of multiple molecules (i.e., single transmission).

2) We derive the *net* number of adsorbed molecules expected at the surface of the A&D receiver in any time duration. To measure the equilibrium concentration for a single transmission, we also derive the asymptotic number of *cumulative* adsorbed molecules expected at the surface of A&D receiver as time goes to infinity.

3) Unlike [20], where the received signal is demodulated based on the total number of molecules expected at the passive receiver, we consider a simple demodulator based on the net number of adsorbed molecules

expected. When multiple bits are transmitted, the net number is more consistent than the total number.

4) We apply the Skellam distribution to approximate the net number of adsorbed molecules expected at the surface of the A&D receiver due to a single transmission of molecules. We formulate the bit error probability of the A&D receiver using the Skellam distribution. Our results show the positive effect of adsorption rate and negative effect of desorption rate on the error probability of A&D receiver with last transmit bit-1.

5) We propose a simulation algorithm to simulate the diffusion, adsorption and desorption behavior of information molecules based on a particle-based simulation framework. Unlike existing simulation platforms (e.g., Smoldyn [32], N3sim [33]), our simulation algorithm captures the dynamic processes of the MC system, which includes the signal modulation, molecule free diffusion, molecule A&D at the surface of the receiver, and signal demodulation. Our simulation results are in close agreement with the derived number of adsorbed molecules expected. Interestingly, we demonstrate that the error probability of the A&D receiver for the last transmitted bit is worse at higher detection thresholds but better at low detection thresholds than both the full adsorption and partial adsorption receivers. This is because the A&D receiver observes a lower peak number of adsorbed molecules but then a faster decay.

The rest of this paper is organized as follows. In Section II, we introduce the system model with a single transmission at the transmitter and the A&D receiver. In Section III, we present the channel impulse response of information molecules, i.e., the exact and asymptotic number of adsorbed molecules expected at the surface of the receiver. In Section IV, we derive the bit error probability of the proposed MC model due to multiple symbol intervals. In Section V, we present the simulation framework. In Section VI, we discuss the numerical and simulation results. In Section VII, we conclude the contributions of this paper.

II. SYSTEM MODEL

We consider a 3-dimensional (3D) diffusion-based MC system in a fluid environment with a point transmitter and a spherical A&D receiver. We assume spherical symmetry where the transmitter is *effectively* a spherical shell and the molecules are released from random points over the shell; the actual angle to the transmitter when a molecule hits the receiver is ignored, so this assumption cannot accommodate a flowing environment. The point transmitter is located at a distance r_0 from the center of the receiver and is at a distance $d = r_0 - r_r$ from the nearest point on the surface of the receiver with radius r_r. The extension to an asymmetric spherical model that accounts for the actual angle to the transmitter when a molecule hits the receiver complicates the derivation of the channel impulse response, and might be solved following [34].

We assume all receptors are equivalent and can accommodate at most one adsorbed molecule. The ability of a molecule to adsorb at a given site is independent of the occupation of neighboring receptors. The spherical receiver is assumed to have no physical limitation on the number or placement of receptors on the receiver. Thus, there is no limit on the number of molecules adsorbed to the receiver surface (i.e., we ignore saturation). This is an appropriate assumption for a sufficiently low number of adsorbed molecules, or for a sufficiently high concentration of receptors.

Once an information molecule binds to a receptor site, a physical response is activated to facilitate the counting of the molecule. Generally, due to the non-covalent nature of binding, in the dissociation process, the receptor may release the adsorbed molecule to the fluid environment without changing its physical characteristics, e.g., a ligand-binding receptor [35]. We also assume perfect synchronization between the transmitter and the receiver as in [10]–[12], [14]–[18], and [20]. The system includes five processes: emission, propagation, reception, modulation and demodulation, which are detailed in the following.

A. Emission

The point transmitter releases one type of information molecule (e.g., hormones, pheromones) to the receiver for information transmission. The transmitter emits the information molecules at $t = 0$, where we define the initial condition as [26, eq. (3.61)]

$$C(r, t \to 0|r_0) = \frac{1}{4\pi r_0^2}\delta(r - r_0), \tag{1}$$

where $C(r, t \to 0|r_0)$ is the molecule distribution function at time $t \to 0$ and distance r with initial distance r_0.

We also define the first boundary condition as

$$\lim_{r \to \infty} C(r, t|r_0) = 0, \tag{2}$$

such that at arbitrary time, the molecule distribution function equals zero when r goes to infinity.

B. Diffusion

Once the information molecules are emitted, they diffuse by randomly colliding with other molecules in the environment. This random motion is called Brownian motion [6]. The concentration of information molecules is assumed to be sufficiently low that the collisions between those information molecules are ignored [6], such that each information molecule diffuses independently with constant diffusion coefficient D. The propagation model in a 3D environment is described by Fick's second law [6], [15]:

$$\frac{\partial(r \cdot C(r, t|r_0))}{\partial t} = D\frac{\partial^2(r \cdot C(r, t|r_0))}{\partial r^2}, \tag{3}$$

where the diffusion coefficient is usually obtained via experiment [36].

C. Reception

We consider a reversible A&D receiver that is capable of counting the net number of adsorbed molecules at the surface of the receiver. Any molecule that hits the receiver surface is either adsorbed to the receiver surface or reflected back

into the fluid environment, based on the adsorption rate k_1 (length$\times$time^{-1}). The adsorbed molecules either desorb or remain stationary at the surface of receiver, based on the desorption rate k_{-1} (time^{-1}).

At $t = 0$, there are no information molecules at the receiver surface, so the second initial condition is

$$C(r_r, 0|r_0) = 0, \text{ and } C_a(0|r_0) = 0, \tag{4}$$

where $C_a(t|r_0)$ is the average concentration of molecules that are adsorbed to the receiver surface at time t.

For the solid-fluid interface located at r_r, the second boundary condition of the information molecules is [31, eq. (4)]

$$D\frac{\partial(C(r, t|r_0))}{\partial r}\bigg|_{r=r_r^+} = k_1 C(r_r, t|r_0) - k_{-1} C_a(t|r_0), \tag{5}$$

which accounts for the adsorption and desorption reactions that can occur at the surface of the receiver.

Most generally, when both k_1 and k_{-1} are non-zero finite constants, (5) is the boundary condition for the A&D receiver. When $k_1 \to \infty$ and $k_{-1} = 0$, (5) is the boundary condition for the full adsorption (or fully-adsorbing) receiver, whereas when k_1 is a non-zero finite constant and $k_{-1} = 0$, (5) is the boundary condition for the partial adsorption (or partially-adsorbing) receiver. In these two special cases with $k_{-1} = 0$, the lack of desorption results in more effective adsorption. Here, the adsorption rate k_1 is approximately limited to the thermal velocity of potential adsorbents (e.g., $k_1 < 7 \times 10^6 \, \mu\text{m/s}$ for a 50 kDa protein at 37 °C) [31]; the desorption rate k_{-1} is typically between $10^{-4} \, \text{s}^{-1}$ and $10^4 \, \text{s}^{-1}$ [37].

The surface concentration $C_a(t|r_0)$ changes over time as follows:

$$\frac{\partial C_a(t|r_0)}{\partial t} = D\frac{\partial(C(r, t|r_0))}{\partial r}\bigg|_{r=r_r^+}, \tag{6}$$

which shows that the change in the adsorbed concentration over time is equal to the flux of diffusion molecules towards the surface.

Combining (5) and (6), we write

$$\frac{\partial C_a(t|r_0)}{\partial t} = k_1 C(r_r, t|r_0) - k_{-1} C_a(t|r_0), \tag{7}$$

which is known as the Robin or radiation boundary condition [38], [39] and shows that the equivalent adsorption rate is proportional to the molecule concentration at the surface.

D. Modulation and Demodulation

In this model, we consider the widely applied amplitude-based modulation—concentration shift keying (CSK) [14], [16], [18], [40], [41], where the concentration of information molecules is interpreted as the amplitude of the signal. Specifically, we utilize Binary CSK, where the transmitter emits N_1 molecules at the start of the bit interval to represent the transmit bit-1, and emits N_2 molecules at the start of the bit interval to represent the transmit bit-0. To reduce the energy consumption and make the received signal more distinguishable, we assume that $N_1 = N_{\text{tx}}$ and $N_2 = 0$.

We assume that the receiver is able to count the *net* number of information molecules that are adsorbed to the surface of the receiver in any sampling period by subtracting the number of molecules bound to the surface of the receiver at the end of previous sampling time from that at the end of current sampling time. The net number of adsorbed molecules over a bit interval is then demodulated as the received signal for that bit interval. This approach is in contrast to [18], where the cumulative number of molecule arrivals in each symbol duration was demodulated as the received signal (i.e., cumulative counter is reset to zero at each symbol duration). We claim (and our results will demonstrate) that our approach is more appropriate for a simple demodulator. Here, we write the net number of adsorbed molecules measured by the receiver in the jth bit interval as $N_{\text{new}}^{\text{Rx}}[j]$, and the decision threshold for the number of received molecules is N_{th}. Using threshold-based demodulation, the receiver demodulates the received signal as bit-1 if $N_{\text{new}}^{\text{Rx}}[j] \geq N_{\text{th}}$, and demodulates the received signal as bit-0 if $N_{\text{new}}^{\text{Rx}}[j] < N_{\text{th}}$.

III. RECEIVER OBSERVATIONS

In this section, we first derive the spherically-symmetric spatial distribution $C(r, t|r_0)$, which is the probability of finding a molecule at distance r and time t. We then derive the flux at the surface of the A&D receiver, from which we derive the exact and asymptotic number of adsorbed molecules expected at the surface of the receiver.

A. Exact Results

The time-varying spatial distribution of information molecules at the surface of the receiver is an important statistic for capturing the molecule concentration in the diffusion-based MC system. We solve it in the following theorem.

Theorem 1: The expected time-varying spatial distribution of an information molecule released into a 3D fluid environment with a reversible adsorbing receiver is given by

$$C(r, t|r_0) = \frac{1}{8\pi r_0 r\sqrt{\pi Dt}} \exp\left\{-\frac{(r-r_0)^2}{4Dt}\right\}$$
$$+ \frac{1}{8\pi r_0 r\sqrt{\pi Dt}} \exp\left\{-\frac{(r+r_0-2r_r)^2}{4Dt}\right\}$$
$$- \frac{1}{2\pi r} \int_0^\infty \left(e^{-jwt}\varphi_Z^*(w) + e^{jwt}\varphi_Z(w)\right)\mathrm{d}w, \tag{8}$$

where

$$\varphi_Z(w) = Z(jw) = \frac{2\left(\frac{1}{r_r} + \frac{k_1 jw}{D(jw+k_{-1})}\right)}{\left(\frac{1}{r_r} + \frac{k_1 jw}{D(jw+k_{-1})} + \sqrt{\frac{jw}{D}}\right)}$$
$$\times \frac{1}{8\pi r_0\sqrt{Djw}} \exp\left\{-(r+r_0-2r_r)\sqrt{\frac{jw}{D}}\right\}, \tag{9}$$

and $\varphi_Z^*(w)$ is the complex conjugate of $\varphi_Z(w)$.

Proof: See the Appendix. ∎

Our results in **Theorem 1** can be easily computed using Matlab. We observe that (8) reduces to an *absorbing* receiver [26, eq. (3.99)] when there is no desorption (i.e., $k_{-1} = 0$).

To characterize the number of information molecules adsorbed to the surface of the receiver using $C(r, t|r_0)$, we define the rate of the coupled reaction (i.e., adsorption and desorption) at the surface of the A&D receiver as [26, eq. (3.106)]

$$K(t|r_0) = 4\pi r_r^2 D \frac{\partial C(r, t|r_0)}{\partial r}\bigg|_{r=r_r}. \quad (10)$$

Corollary 1: The rate of the coupling reaction at the surface of a reversible adsorbing receiver is given by

$$K(t|r_0) = 2r_r D \int_0^\infty e^{-jwt} \left[\sqrt{\frac{jw}{D}}\varphi_Z(w)\right]^* dw$$
$$+ 2r_r D \int_0^\infty e^{jwt} \left[\sqrt{\frac{jw}{D}}\varphi_Z(w)\right] dw, \quad (11)$$

where $\varphi_Z(w)$ is as given in (9).

Proof: By substituting (8) into (10), we derive the coupling reaction rate at the surface of an A&D receiver as (11). ∎

From **Corollary 1**, we can derive the net change in the number of adsorbed molecules expected for any time interval in the following theorem.

Theorem 2: With a single emission at $t = 0$, the net change in the number of adsorbed molecules expected at the surface of the A&D receiver during the interval $[T, T+T_s]$ is derived as

$$\mathbb{E}\left[N_{\text{A\&D}}\left(\Omega_{r_r}, T, T+T_s|r_0\right)\right] = 2r_r N_{\text{tx}} D$$
$$\times \left[\int_0^\infty \frac{e^{-jwT} - e^{-jw(T+T_s)}}{jw} \left[\sqrt{\frac{jw}{D}}\varphi_Z(w)\right]^* dw\right.$$
$$\left.+ \int_0^\infty \frac{e^{jw(T+T_s)} - e^{jwT}}{jw} \left[\sqrt{\frac{jw}{D}}\varphi_Z(w)\right] dw\right], \quad (12)$$

where $\varphi_Z(w)$ is given in (9), T_s is the sampling time, and Ω_{r_r} represents the spherical receiver with radius r_r.

Proof: The cumulative fraction of particles that are adsorbed to the receiver surface at time T is expressed as

$$R_{\text{A\&D}}\left(\Omega_{r_r}, T|r_0\right) = \int_0^T K(t|r_0)dt$$
$$= 2r_r D \left[\int_0^\infty \frac{1 - e^{-jwT}}{jw} \left[\sqrt{\frac{jw}{D}}\varphi_Z(w)\right]^* dw\right.$$
$$\left.+ \int_0^\infty \frac{e^{jwT} - 1}{jw} \left[\sqrt{\frac{jw}{D}}\varphi_Z(w)\right] dw\right]. \quad (13)$$

Based on (13), the net change in adsorbed molecules expected at the receiver surface during the interval $[T, T+T_s]$ is defined as

$$\mathbb{E}\left[N_{\text{A\&D}}\left(\Omega_{r_r}, T, T+T_s|r_0\right)\right]$$
$$= N_{\text{tx}} R_{\text{A\&D}}\left(\Omega_{r_r}, T+T_s|r_0\right) - N_{\text{tx}} R_{\text{A\&D}}\left(\Omega_{r_r}, T|r_0\right). \quad (14)$$

Substituting (13) into (14), we derive the expected net change of adsorbed molecules during any observation interval as (12). ∎

Note that the net change in the number of adsorbed molecules in each *bit interval* will be recorded at the receiver, which will be converted to the recorded net change of adsorbed molecules in each *bit interval*, and compared with the decision threshold N_{th} to demodulate the received signal (the sampling interval is smaller than one bit interval).

B. Asymptotic Behavior: Equilibrium Concentration

In this section, we are interested in the asymptotic number of adsorbed molecules due to a single emission as T_b goes to infinity, i.e., the concentration of adsorbed molecules at the steady state. Note that this asymptotic concentration of adsorbed molecules is an important quantity that influences the number of adsorbed molecules expected in subsequent bit intervals, and we have assumed that the receiver surface has infinite receptors. Thus, in the remainder of this section, we derive the cumulative number of adsorbed molecules expected at the surface of the A&D receiver, the partial adsorption receiver, and the full adsorption receiver, as $T_b \to \infty$.

1) Reversible A&D Receiver:

Lemma 1: As $T_b \to \infty$, the cumulative number of adsorbed molecules expected at the A&D receiver simplifies to

$$\mathbb{E}\left[N_{\text{A\&D}}\left(\Omega_{r_r}, T_b \to \infty|r_0\right)\right] = \frac{N_{\text{tx}} r_r}{2r_0}$$
$$- 4N_{\text{tx}} r_r D \int_0^\infty \frac{1}{w}\text{Im}\left[\sqrt{\frac{jw}{D}}\varphi_Z(w)\right]dw. \quad (15)$$

Proof: We express the cumulative fraction of particles adsorbed to the surface of the A&D receiver at time T_b in (13) as

$$R_{\text{A\&D}}\left(\Omega_{r_r}, T_b|r_0\right)$$
$$= \text{Re}\left[4r_r D \int_0^\infty \frac{e^{jwT_b} - 1}{jw}\left(\sqrt{\frac{jw}{D}}\varphi_Z(w)\right)dw\right]$$
$$= 4r_r D \int_0^\infty \frac{\sin wT_b}{w}\text{Re}\left[\sqrt{\frac{jw}{D}}\varphi_Z(w)\right]dw$$
$$+ 4r_r D \int_0^\infty \frac{\cos wT_b - 1}{w}\text{Im}\left[\sqrt{\frac{jw}{D}}\varphi_Z(w)\right]dw$$
$$= 4r_r D \int_0^\infty \frac{\sin z}{z}\text{Re}\left[q\left(\frac{z}{T_b}\right)\right]dz + 4r_r D \int_0^\infty \frac{\cos z}{z}$$
$$\times \text{Im}\left[q\left(\frac{z}{T_b}\right)\right]dz - 4r_r D \int_0^\infty \frac{1}{w}\text{Im}[q(w)]dw, \quad (16)$$

where

$$q(w) = \frac{\left(\frac{1}{r_r} + \frac{k_1 jw}{D(jw+k_{-1})}\right)}{\left(\frac{1}{r_r} + \frac{k_1 jw}{D(jw+k_{-1})} + \sqrt{\frac{jw}{D}}\right)}\frac{1}{4\pi r_0 D}$$
$$\times \exp\left\{-(r_0 - r_r)\sqrt{\frac{jw}{D}}\right\}. \quad (17)$$

As $T_b \to \infty$, we have the following:

$$
\begin{aligned}
&\mathbb{E}\big[N_{\mathrm{A\&D}}\big(\Omega_{r_r}, T_b \to \infty|r_0\big)\big] \\
&= 4r_r D N_{\mathrm{tx}}\bigg[\int_0^\infty \frac{\sin z}{z}\mathrm{Re}\big[q(0)\big]dz \\
&\quad + \int_0^\infty \frac{\cos z}{z}\mathrm{Im}\big[q(0)\big]dz - \int_0^\infty \frac{1}{w}\mathrm{Im}\big[q(w)\big]dw\bigg] \\
&\overset{(b)}{=} 4r_r D N_{\mathrm{tx}}\bigg[\int_0^\infty \frac{\sin z}{z}\mathrm{Re}\big[q(0)\big]dz - \int_0^\infty \frac{1}{w}\mathrm{Im}\big[q(w)\big]dw\bigg] \\
&\overset{(c)}{=} N_{\mathrm{tx}}\bigg[\frac{r_r}{\pi r_0}\int_0^\infty \frac{\sin z}{z}dz - 4r_r D\int_0^\infty \frac{1}{w}\mathrm{Im}\big[q(w)\big]dw\bigg] \\
&= \frac{N_{\mathrm{tx}}r_r}{2r_0} - 4N_{\mathrm{tx}}r_r D\int_0^\infty \frac{1}{w}\mathrm{Im}\bigg[\sqrt{\frac{jw}{D}}\varphi_Z(w)\bigg]dw, \quad (18)
\end{aligned}
$$

where (b) is due to the fact that $\mathrm{Im}[q(0)] = 0$, and (c) is due to $q(0) = \frac{1}{4\pi r_0 D}$.

2) Partial Adsorption Receiver: The partial adsorption receiver only adsorbs some of the molecules that collide with its surface, corresponding to k_1 as a finite constant and $k_{-1} = 0$ in (5).

Proposition 1: The number of molecules expected to be adsorbed to the partial adsorption receiver by time T_b, as $T_b \to \infty$, is derived as

$$
\mathbb{E}\big[N_{\mathrm{PA}}\big(\Omega_{r_r}, T_b \to \infty|r_0\big)\big] = \frac{N_{\mathrm{tx}}k_1 r_r^2}{r_0(k_1 r_r + D)}. \quad (19)
$$

Proof: We note that the exact expression for the net number of adsorbed molecules expected at the partial adsorption receiver during $[T, T+T_s]$ can be derived from [26, eq. (3.114)] as

$$
\begin{aligned}
\mathbb{E}\big[N_{\mathrm{PA}}\big(\Omega_{r_r}, T, T+T_s|r_0\big)\big] = N_{\mathrm{tx}}\frac{r_r\alpha - 1}{r_0\alpha} \\
\times\bigg[\mathrm{erf}\bigg\{\frac{r_r - r_0}{\sqrt{4D(T+T_s)}}\bigg\} \\
- \exp\big\{(r_0 - r_r)\alpha + D(T+T_s)\alpha^2\big\} \\
\times \mathrm{erfc}\bigg\{\frac{r_0 - r_r + 2D\alpha(T+T_s)}{\sqrt{4D(T+T_s)}}\bigg\} \\
- \mathrm{erf}\bigg\{\frac{r_r - r_0}{\sqrt{4DT}}\bigg\} + \exp\big\{(r_0 - r_r)\alpha + DT\alpha^2\big\} \\
\times \mathrm{erfc}\bigg\{\frac{r_0 - r_r + 2D\alpha T}{\sqrt{4DT}}\bigg\}\bigg], \quad (20)
\end{aligned}
$$

where $\alpha = \frac{k_1}{D} + \frac{1}{r_r}$.

The cumulative fraction of molecules adsorbed at the partial adsorption receiver by time T_b was derived in [26, eq. (3.114)] as

$$
\begin{aligned}
R_{\mathrm{PA}}(\Omega_r, T_b|r_0) = \frac{r_r\alpha - 1}{r_0\alpha} \\
\times \bigg(1 + \mathrm{erf}\bigg\{\frac{r_r - r_0}{\sqrt{4DT_b}}\bigg\} - \exp\big\{(r_0 - r_r)\alpha + DT_b\alpha^2\big\} \\
\times \mathrm{erfc}\bigg\{\frac{r_0 - r_r + 2D\alpha T_b}{\sqrt{4DT_b}}\bigg\}\bigg). \quad (21)
\end{aligned}
$$

By setting $T_b \to \infty$ and taking the expectation of (21), we arrive at (19). ∎

The asymptotic result in (19) for the partial adsorption receiver reveals that the number of adsorbed molecules expected at infinite time T_b increases with increasing adsorption rate k_1, and decreases with increasing diffusion coefficient D and increasing distance between the transmitter and the center of the receiver r_0.

3) Full Adsorption Receiver: In the full adsorption receiver, all molecules adsorb when they collide with its surface, which corresponds to the case of $k_1 \to \infty$ and $k_{-1} = 0$ in (5).

Proposition 2: The cumulative number of adsorbed molecules expected at the full adsorption receiver by time T_b, as $T_b \to \infty$, is derived as

$$
\mathbb{E}\big[N_{\mathrm{FA}}\big(\Omega_{r_r}, T_b \to \infty|r_0\big)\big] = \frac{N_{\mathrm{tx}}r_r}{r_0}. \quad (22)
$$

Proof: We note that the exact expression for the net number of adsorbed molecules expected at the full adsorption receiver during $[T, T+T_s]$ has been derived in [15] and [26] as

$$
\begin{aligned}
&\mathbb{E}\big[N_{\mathrm{FA}}\big(\Omega_{r_r}, T, T+T_s|r_0\big)\big] \\
&= N_{\mathrm{tx}}\frac{r_r}{r_0}\bigg[\mathrm{erfc}\bigg\{\frac{r_0 - r_r}{\sqrt{4D(T+T_s)}}\bigg\} - \mathrm{erfc}\bigg\{\frac{r_0 - r_r}{\sqrt{4DT}}\bigg\}\bigg]. \quad (23)
\end{aligned}
$$

The fraction of molecules adsorbed to the full adsorption receiver by time T_b was derived in [15, eq. (32)] and [26, eq. (3.116)] as

$$
R_{\mathrm{FA}}(\Omega_r, T_b|r_0) = \frac{r_r}{r_0}\mathrm{erfc}\bigg\{\frac{r_0 - r_r}{\sqrt{4DT_b}}\bigg\}. \quad (24)
$$

By setting $T_b \to \infty$ and taking the expectation of (24), we arrive at (22). ∎

Alternatively, with the help of integration by parts, the result in (15) reduces to the asymptotic result in (22) for the full adsorption receiver by setting $k_1 = \infty$ and $k_{-1} = 0$.

The asymptotic result for the full adsorption receiver in (22) reveals that the cumulative number of adsorbed molecules expected by infinite time T_b is *independent* of the diffusion coefficient, and directly proportional to the ratio between the radius of receiver and the distance between the transmitter and the center of receiver.

IV. ERROR PROBABILITY

In this section, we propose that the net number of adsorbed molecules in a bit interval be used for receiver demodulation. We also derive the error probability of the MC system using the Poisson approximation and the Skellam distribution.

To calculate the error probability at the receiver, we first need to model the statistics of molecule adsorption. For a single emission at $t = 0$, the net number of molecules adsorbed during $[T, T+T_b]$ is *approximately* modeled as the difference between two binomial distributions as

$$
\begin{aligned}
N_{\mathrm{new}}^{\mathrm{Rx}} \sim B\big(N_{\mathrm{tx}}, R_{\mathrm{A\&D}}\big(\Omega_{r_r}, T+T_b|r_0\big)\big) \\
- B\big(N_{\mathrm{tx}}, R_{\mathrm{A\&D}}\big(\Omega_{r_r}, T|r_0\big)\big), \quad (25)
\end{aligned}
$$

where the cumulative fraction of particles that are adsorbed to the A&D receiver $R_{\mathrm{A\&D}}(\Omega_{r_r}, T|r_0)$ is given in (16). Note that

the number of molecules adsorbed at $T+T_b$ depends on that at T, however this dependence can be ignored for a sufficiently large bit interval, and makes (25) accurate. The number of adsorbed molecules represented by Binomial distribution can also be approximated using either the Poisson distributions or the Normal distributions.

The net number of adsorbed molecules depends on the emission in the current bit interval and those in previous bit intervals. Unlike the full adsorption receiver in [18], [42], and [43] and partial adsorption receiver where the net number of adsorbed molecules is always positive, the net number of adsorbed molecules of the A&D receiver *can be negative*. Thus, we cannot model the net number of adsorbed molecules of the reversible adsorption receiver during one bit interval as $N_{\text{new}}^{\text{Rx}} \sim B(N_{\text{tx}}, R(\Omega_{r_r}, T, T+T_b|r_0))$ with $R(\Omega_{r_r}, T, T+T_b|r_0) = \int_{T}^{T+T_b} K(t|r_0)dt$, which was used to model that of full adsorption receiver and partial adsorption receiver [42], [43].

For multiple emissions, the cumulative number of adsorbed molecules is modeled as the sum of multiple binomial random variables. This sum does not lend itself to a convenient expression. Approximations for the sum were used in [44]. Here, the binomial distribution can be approximated with the Poisson distribution, when we have sufficiently large N_{tx} and sufficiently small $R_{\text{A&D}}(\Omega_{r_r}, T|r_0)$ [45]. Thus, we approximate the net number of adsorbed molecules received in the jth bit interval as

$$
\begin{aligned}
N_{\text{new}}^{\text{Rx}}[j] \sim\ & P\left(\sum_{i=1}^{j} N_{\text{tx}} s_i R_{\text{A&D}}\big(\Omega_{r_r}, (j-i+1)T_b|r_0\big)\right) \\
& - P\left(\sum_{i=1}^{j} N_{\text{tx}} s_i R_{\text{A&D}}\big(\Omega_{r_r}, (j-i)T_b|r_0\big)\right),
\end{aligned} \quad (26)
$$

where s_i is the ith transmitted bit. The difference between two Poisson random variables follows the Skellam distribution [46]. For threshold-based demodulation, the error probability of the transmit bit-1 signal in the jth bit is then

$$
\begin{aligned}
P_e\big[\hat{s}_j = 0\big|s_j = 1, s_{1:j-1}\big] \\
= \Pr\big(N_{\text{new}}^{\text{Rx}}[j] < N_{\text{th}}\big|s_j = 1, s_{1:j-1}\big) \\
\approx \sum_{n=-\infty}^{N_{\text{th}}-1} \exp\{-(\Psi_1 + \Psi_2)\}(\Psi_1/\Psi_2)^{n/2} I_n\big(2\sqrt{\Psi_1 \Psi_2}\big),
\end{aligned} \quad (27)
$$

where

$$
\Psi_1 = \sum_{i=1}^{j} N_{\text{tx}} s_i R_{\text{A&D}}\big(\Omega_{r_r}, (j-i+1)T_b|r_0\big), \quad (28)
$$

$$
\Psi_2 = \sum_{i=1}^{j-1} N_{\text{tx}} s_i R_{\text{A&D}}\big(\Omega_{r_r}, (j-i)T_b|r_0\big), \quad (29)
$$

$\hat{s}_j$ is the detected jth bit, and $I_n(\cdot)$ is the modified Bessel function of the first kind.

Similarly, the error probability of the transmit bit-0 signal in the jth bit is given as

$$
\begin{aligned}
P_e\big[\hat{s}_j = 1\big|s_j = 0, s_{1:j-1}\big] \\
= \Pr\big(N_{\text{new}}^{\text{Rx}}[j] \geq N_{\text{th}}\big|s_j = 0, s_{1:j-1}\big) \\
\approx \sum_{n=N_{\text{th}}}^{\infty} \exp\{-(\Psi_1 + \Psi_2)\}(\Psi_1/\Psi_2)^{n/2} I_n\big(2\sqrt{\Psi_1 \Psi_2}\big),
\end{aligned} \quad (30)
$$

where Ψ_1 and Ψ_1 are given in (28) and (29), respectively.

Thus, the error probability of the random transmit bit in the jth interval is expressed by

$$
\begin{aligned}
P_e[j] = P_1 P_e\big[\hat{s}_j = 0\big|s_j = 1, s_{1:j-1}\big] \\
+ P_0 P_e\big[\hat{s}_j = 1\big|s_j = 0, s_{1:j-1}\big],
\end{aligned} \quad (31)
$$

where P_1 and P_0 denotes the probability of sending bit-1 and bit-0, respectively.

For comparison, we also present the error probability of the transmit bit-1 signal in the jth bit and error probability of the transmit bit-0 signal in the jth bit for the full adsorption receiver and the partial adsorption receiver using the Poisson approximation as

$$
P_e\big[\hat{s}_j = 0\big|s_j = 1, s_{1:j-1}\big] \approx \exp\{N_{\text{tx}}\Gamma\} \sum_{n=0}^{N_{\text{th}}-1} \frac{[N_{\text{tx}}\Gamma]^n}{n!}, \quad (32)
$$

and

$$
P_e\big[\hat{s}_j = 1\big|s_j = 0, s_{1:j-1}\big] \approx 1 - \exp\{N_{\text{tx}}\Gamma\} \sum_{n=0}^{N_{\text{th}}-1} \frac{[N_{\text{tx}}\Gamma]^n}{n!}. \quad (33)
$$

In (32) and (33), we have

$$
\Gamma = \sum_{i=1}^{j} s_i R_{\text{FA}}\big(\Omega_{r_r}, (j-i)T_b, (j-i+1)T_b|r_0\big) \quad (34)
$$

for the full adsorption receiver, and

$$
\Gamma = \sum_{i=1}^{j} s_i R_{\text{PA}}\big(\Omega_{r_r}, (j-i)T_b, (j-i+1)T_b|r_0\big) \quad (35)
$$

for the partial adsorption receiver.

V. SIMULATION FRAMEWORK

This section describes the stochastic simulation framework for the point-to-point MC system with the A&D receiver described by (5), which can be simplified to the MC system with the partial adsorption receiver and full adsorption receiver by setting $k_{-1} = 0$ and $k_1 = \infty$, respectively. This simulation framework takes into account the signal modulation, molecule free diffusion, molecule A&D at the surface of the receiver, and signal demodulation.

To model the stochastic reaction of molecules in the fluid, two options are a subvolume-based simulation framework or a particle-based simulation framework. In a subvolume-based simulation framework, the environment is divided into many subvolumes, where the number of molecules in each subvolume is recorded [25]. In a particle-based simulation framework [47], the exact position of each molecule

Algorithm 1 The Simulation of a MC System With an A&D Receiver

---

Require: N_{tx}, r_0, r_r, Ω_{r_r}, D, Δt, T_s, T_b, N_{th}

1: **procedure** INITIALIZATION
2:      Generate Random Bit Sequence $\{b_1, b_2, \cdots, b_j, \cdots\}$
3:      Determine Simulation End Time
4: **For all** Simulation Time Step **do**
5: **If** at start of jth bit interval and b_j = "1"
6:      Add N_{tx} emitted molecules
7: **For all** free molecules in environment **do**
8:      Propagate free molecules following $\mathcal{N}(0, 2D\Delta t)$
9:      Evaluate distance d_m of molecule to receiver
10:     **if** $d_m < r_r$ **then**
11:         Update state & location of collided molecule
12:         Update # of collided molecules N_C
13: **For all** N_C collided molecules **do**
14:     **if** Adsorption Occurs **then**
15:         Update # of *newly*-adsorbed molecules N_A
16:         Calculate adsorbed molecule location
17:         (x_m^A, y_m^A, z_m^A)
18:     **else**
19:         Reflect the molecule off receiver surface to
20:         $(x_m^{Bo}, y_m^{Bo}, z_m^{Bo})$
21: **For all** *previously*-adsorbed molecules **do**
22:     **if** Desorption Occurs **then**
23:         Update state & location of desorbed molecule
24:         Update # of *newly*-desorbed molecules N_D
25:         Displace *newly*-desorbed molecule to
26:         (x_m^D, y_m^D, z_m^D)
27:     Calculate *net* number of adsorbed molecules,
28:     which is $N_A - N_D$
29: Add net number of adsorbed molecules in each simulation interval of jth bit interval to determine $N_{new}^{Rx}[j]$
30: Demodulate by comparing $N_{new}^{Rx}[j]$ with N_{th}

---

and the number of molecules in the fluid environment is recorded. To accurately capture the locations of individual information molecules, we adopt a particle-based simulation framework with a spatial resolution on the order of several nanometers [47].

A. Algorithm

We present the algorithm for simulating the MC system with an A&D receiver in Algorithm 1. In the following subsections, we describe the details of Algorithm 1.

B. Modulation, Emission, and Diffusion

In our model, we consider BCSK, where two different numbers of molecules represent the binary signals "1" and "0". At the start of each bit interval, if the current bit is "1", then N_{tx} molecules are emitted from the point transmitter at a distance r_0 from the center of the receiver. Otherwise, the point transmitter emits no molecules to transmit bit-0.

The time is divided into small simulation intervals of size Δt, and each time instant is $t_m = m\Delta t$, where m is the current

simulation index. According to Brownian motion, the displacement of a molecule in each dimension in one simulation step Δt can be modeled by an independent Gaussian distribution with variance $2D\Delta t$ and zero mean $\mathcal{N}(0, 2D\Delta t)$. The displacement ΔS of a molecule in a 3D fluid environment in one simulation step Δt is therefore

$$\Delta S = \{\mathcal{N}(0, 2D\Delta t),\ \mathcal{N}(0, 2D\Delta t),\ \mathcal{N}(0, 2D\Delta t)\}. \quad (36)$$

In each simulation step, the number of molecules and their locations are stored.

C. Adsorption or Reflection

According to the second boundary condition in (6), molecules that collide with the receiver surface are either adsorbed or reflected back. The N_C collided molecules are identified by calculating the distance between each molecule and the center of the receiver. Among the collided molecules, the probability of a molecule being adsorbed to the receiver surface, i.e., the adsorption probability, is a function of the diffusion coefficient, which is given as [48, eq. (10)]

$$P_A = k_1 \sqrt{\frac{\pi \Delta t}{D}}. \quad (37)$$

The probability that a collided molecule bounces off of the receiver is $1 - P_A$.

It is known that adsorption may occur during the simulation step Δt, and determining exactly where a molecule adsorbed to the surface of the receiver during Δt is a non-trivial problem. Unlike [31] (which considered a flat adsorbing surface), we assume that the molecule's adsorption site during $[t_{m-1}, t_m]$ is the location where the line, formed by this molecule's location at the start of the current simulation step $(x_{m-1}, y_{m-1}, z_{m-1})$ and this molecule's location at the end of the current simulation step after diffusion (x_m, y_m, z_m), intersects the surface of the receiver. Assuming that the location of the center of receiver is (x_r, y_r, z_r), then the location of the intersection point between this 3D line segment, and a sphere with center at (x_r, y_r, z_r) in the mth simulation step, can be shown to be

$$x_m^A = x_{m-1} + \frac{x_m - x_{m-1}}{\Lambda} g, \quad (38)$$

$$y_m^A = y_{m-1} + \frac{y_m - y_{m-1}}{\Lambda} g, \quad (39)$$

$$z_m^A = z_{m-1} + \frac{z_m - z_{m-1}}{\Lambda} g, \quad (40)$$

where

$$\Lambda = \sqrt{(x_m - x_{m-1})^2 + (y_m - y_{m-1})^2 + (z_m - z_{m-1})^2}, \quad (41)$$

$$g = \frac{-b - \sqrt{b^2 - 4ac}}{2a}. \quad (42)$$

In (42), we have

$$a = \left(\frac{x_m - x_{m-1}}{\Lambda}\right)^2 + \left(\frac{y_m - y_{m-1}}{\Lambda}\right)^2 + \left(\frac{z_m - z_{m-1}}{\Lambda}\right)^2,$$

$$b = 2\frac{(x_m - x_{m-1})(x_{m-1} - x_r)}{\Lambda} + 2\frac{(y_m - y_{m-1})(y_{m-1} - y_r)}{\Lambda}$$

$$+ 2\frac{(z_m - z_{m-1})(z_{m-1} - z_r)}{\Lambda}, \quad (43)$$

$$c = (x_{m-1} - x_r)^2 + (y_{m-1} - y_r)^2 + (z_{m-1} - z_r)^2 - r_r{}^2,$$
$$(44)$$

where Λ is given in (41).

Of course, due to symmetry, the location of the adsorption site does not impact the overall accuracy of the simulation.

If a molecule fails to adsorb to the receiver, then in the reflection process we make the approximation that the molecule bounces back to its position at the start of the current simulation step. Thus, the location of the molecule after reflection by the receiver in the mth simulation step is approximated as

$$\left(x_m^{Bo}, y_m^{Bo}, z_m^{Bo}\right) = (x_{m-1}, y_{m-1}, z_{m-1}). \qquad (45)$$

Note that the approximations for molecule locations in the adsorption process and the reflection process can be accurate for sufficiently small simulation steps (e.g., $\Delta t < 10^{-7}$ s for the system that we simulate in Section V), but small simulation steps result in poor computational efficiency. The tradeoff between the accuracy and the efficiency can be deliberately balanced by the choice of simulation step.

D. Desorption

In the desorption process, the molecules adsorbed at the receiver boundary either desorb or remain adsorbed. The desorption process can be modeled as a first-order chemical reaction. Thus, the desorption probability of a molecule at the receiver surface during Δt is given by [31, eq. (22)]

$$P_D = 1 - e^{-k_{-1}\Delta t}. \qquad (46)$$

The displacement of a molecule after desorption is an important factor for accurate modeling of molecule behaviour. If the simulation step were small, then we might place the desorbed molecule near the receiver surface; otherwise, doing so may result in an artificially higher chance of re-adsorption in the following time step, resulting in an inexact concentration profile. To avoid this, we take into account the diffusion *after* desorption, and place the desorbed molecule away from the surface with displacement $(\Delta x, \Delta y, \Delta z)$

$$(\Delta x, \Delta y, \Delta z) = (f(P_1), f(P_2), f(P_3)), \qquad (47)$$

where each component was empirically found to be [31, eq. (27)]

$$f(P) = \sqrt{2D\Delta t}\,\frac{0.571825P - 0.552246P^2}{1 - 1.53908P + 0.546424P^2}. \qquad (48)$$

In (47), P_1, P_2 and P_3 are uniform random numbers between 0 and 1. Placing the desorbed molecule at a random distance away from where the molecule was adsorbed may not be sufficiently accurate due to the lack of consideration for the coupling effect of A&D and the diffusion coefficient in (48).

Unlike [31], we have a spherical receiver, such that a molecule after desorption in our model must be displaced differently. We assume that the location of a molecule after desorption (x_m^D, y_m^D, z_m^D), based on its location at the start of

the current simulation step and the location of the center of the receiver (x_r, y_r, z_r), can be approximated as

$$x_m^D = x_{m-1}^A + \text{sgn}\left(x_{m-1}^A - x_r\right)\Delta x,$$
$$y_m^D = y_{m-1}^A + \text{sgn}\left(y_{m-1}^A - y_r\right)\Delta y,$$
$$z_m^D = z_{m-1}^A + \text{sgn}\left(z_{m-1}^A - z_r\right)\Delta z. \qquad (49)$$

In (49), Δx, Δy, and Δz are given in (47), and $\text{sgn}(\cdot)$ is the Sign function.

E. Demodulation

The receiver is capable of counting the net change in the number of adsorbed molecules in each bit interval. The net number of adsorbed molecules for an entire bit interval is compared with the threshold N_{th} and demodulated as the received signal.

VI. NUMERICAL RESULTS

In this section, we examine the channel response and the asymptotic channel response due to a single bit transmission. We also examine the channel response and the error probability due to multiple bit transmissions. In all figures of this section, we use FA, PA, "Anal." and "Sim." to abbreviate "Full adsorption receiver", "Partial adsorption receiver", "Analytical" and "Simulation", respectively. Also, the units for the adsorption rate k_1 and desorption rate k_{-1} are μm/s and s^{-1} in all figures, respectively. In Figs. 1 to 4, we set the parameters according to micro-scale cell-to-cell communication[1]: $N_{\text{tx}} = 1000$, $r_r = 10$ μm, $r_0 = 11$ μm, $D = 8$ μm^2/s, and the sampling interval $T_s = 0.002$ s.

A. Channel Response

Figs. 1 and 2 plot the net change of adsorbed molecules at the surface of the A&D receiver during each sampling time T_s due to a single bit transmission. The expected analytical curves are plotted using the exact result in (12). The simulation points are plotted by measuring the net change of adsorbed molecules during $[t, t + T_s]$ using Algorithm 1 described in Section IV, where $t = nT_s$, and $n \in \{1, 2, 3, \ldots\}$. In both figures, we average the net number of adsorbed molecules expected over 10000 independent emissions of $N_{\text{tx}} = 1000$ information molecules at time $t = 0$. We see that the expected net number of adsorbed molecules measured using simulation is close to the exact analytical curves. The small gap between the curves results from the local approximations in the adsorption, reflection, and desorption processes in (37), (45), and (49), which can be reduced by setting a smaller simulation step.

Fig. 1 examines the impact of the adsorption rate on the net number of adsorbed molecules expected at the surface of the receiver. We fix the desorption rate to be $k_{-1} = 5\,\text{s}^{-1}$.

[1]The small separation distance between the transmitter and receiver compared to the receiver radius follows from the example of the pancreatic islets, where the average cell size is around 15 micrometers and the communication range is around 1−15 micrometers [15], [16].
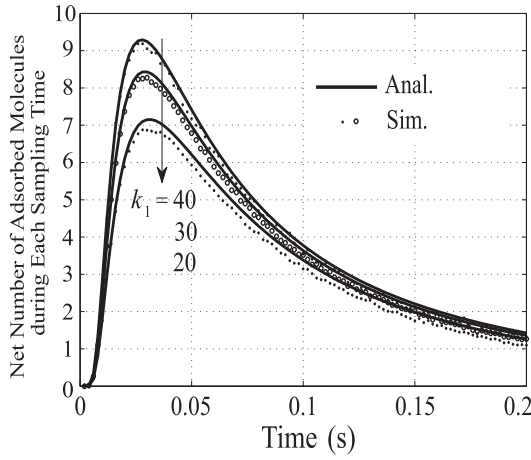
Fig. 1. The net number of adsorbed molecules for various adsorption rates with $k_{-1} = 5$ s^{-1} and the simulation step $\Delta t = 10^{-5}$ s.

Fig. 3. The net number of adsorbed molecules with the simulation step $\Delta t = 10^{-5}$ s.

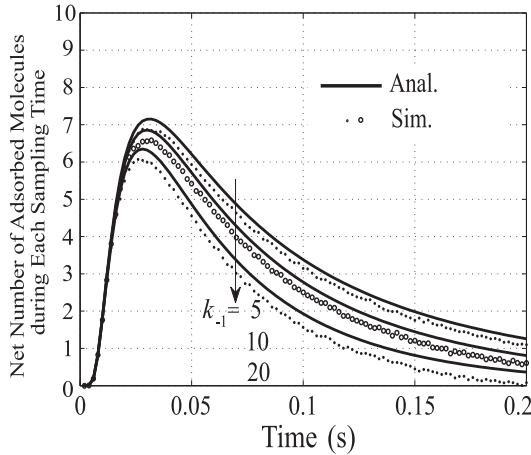

Fig. 2. The net number of adsorbed molecules for various desorption rates with $k_1 = 20 \, \mu$m/s and the simulation step $\Delta t = 10^{-5}$ s.

The expected net number of adsorbed molecules increases with increasing adsorption rate k_1, as predicted by (5). Fig. 2 shows the impact of the desorption rate on the expected net number of adsorbed molecules at the surface of the receiver. We set $k_1 = 20 \, \mu$m/s. The net number of adsorbed molecules expected decreases with increasing desorption rate k_{-1}, which is as predicted by (5). From a communication perspective, Fig. 1 shows that a higher adsorption rate makes the bit-1 signal more distinguishable, whereas Fig. 2 shows that a lower desorption rate makes the bit-1 signal more distinguishable for the decoding process. In Figs. 1 and 2, the shorter tail due to the lower adsorption rate and the higher desorption rate corresponds to less intersymbol interference.

Fig. 3 plots the net number of adsorbed molecules from 1 bit transmission over a longer time scale. We compare the A&D receiver with other receiver designs in order to compare their intersymbol interference (ISI). The analytical curves for the A&D receiver, the partial adsorption receiver, and the full adsorption receiver are plotted using the expressions in (12), (20), and (23), respectively. The markers are plotted by measuring the net number of adsorbed molecules during $[t, t + T_s]$ for one bit interval using Algorithm 1 described in
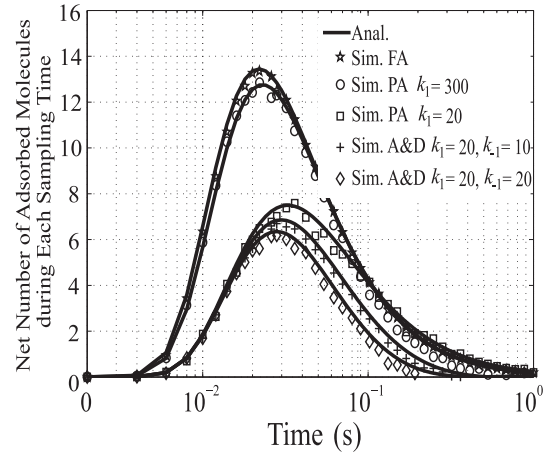
Section IV. We see a close match between the analytical curves and the simulation curves, which confirms the correctness of our derived results.

It is clear from Fig. 3 that the full adsorption receiver and the partial adsorption receiver with high adsorption rate have longer "tails". Interestingly, the A&D receiver in our model has the shorter tail, even though it has the same adsorption rate k_1 as one of the partial adsorption receivers. This might be surprising since the A&D receiver would have more total adsorption events than the partial adsorption receiver with the same k_1. The reason for this difference is that the desorption behaviour at the surface of the receiver results in more adsorption events, but not more *net* adsorbed molecules; molecules that desorb are not counted unless they adsorb again.

As expected, we see the highest peak $\mathbb{E}[N(\Omega_{r_r}, T, T + T_s | r_0)]$ in Fig. 3 for the full adsorption receiver, which is because all molecules colliding with the surface of the receiver are adsorbed. For the partial adsorption receiver, the peak value of $\mathbb{E}[N(\Omega_{r_r}, T, T + T_s | r_0)]$ increases with increasing adsorption rate k_1 as shown in (5). The net number of adsorbed molecules expected at the partial adsorption receiver is higher than that at the A&D receiver with the same k_1. This means the full adsorption receiver and the partial adsorption receiver have more distinguishable received signals between bit-1 and bit-0, compared with the A&D receiver.

B. Equilibrium Concentration

Fig. 4 plots the number of *cumulatively*-adsorbed molecules expected at the surface of the different types of receiver with a single emission N_{tx} and as $T_b \to \infty$. The solid curves are plotted by accumulating the net number of adsorbed molecules expected in each sampling time $\mathbb{E}[N(\Omega_{r_r}, T, T + T_s | r_0)]$ in (14), (20), and (23). The dashed lines are plotted using the derived asymptotic expressions in (15), (19), and (22). The asymptotic analytical lines are in precise agreement with the exact analytical curves as $T_b \to \infty$. The exact analytical curves of the full adsorption receiver and the partial
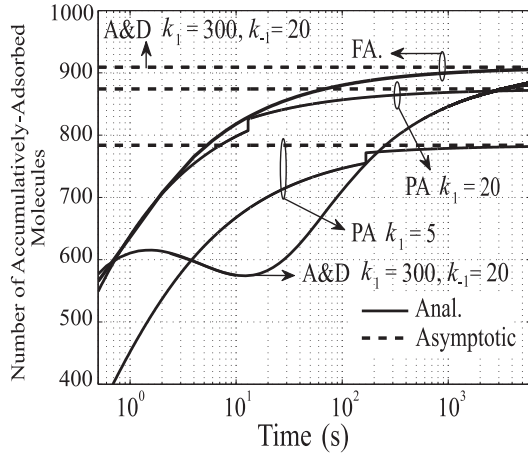
Fig. 4. The cumulative number of adsorbed molecules.
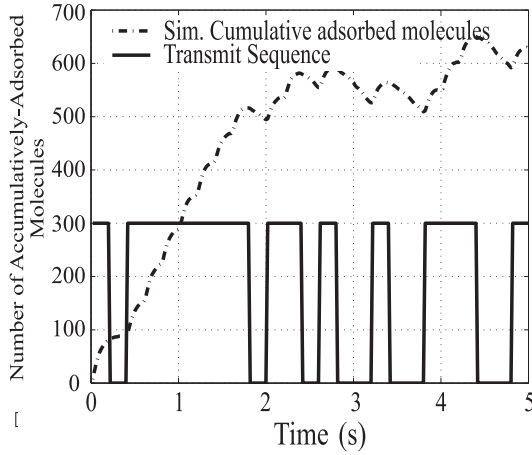

Fig. 6. The net number of adsorbed molecules.

Fig. 5. The cumulative number of adsorbed molecules.

adsorption receiver converge to their own asymptotic analytical lines faster than the convergence of the A&D receiver. Interestingly, we find that the analytical curve of the A&D receiver decreases after increasing over a few bit intervals, and then increases again, while that of the partial adsorption receiver has an increasing trend as time goes large and shows a sudden jump at a specific time. The discontinuities in the PA curves are caused by the underflow during the evaluation of $erfc(x)$, which results from the limitation of Matlab's smallest possible double. As expected, the asymptotic curve of the partial adsorption receiver degrades with decreasing k_1, as shown in (19). More importantly, the full adsorption receiver has a higher initial accumulation rate but the *same* asymptotic number of bound molecules as that of the A&D receiver with $k_1 = 300$ μm/s and $k_{-1} = 20$ s^{-1}.

C. Demodulation Criterion

In Figs. 5 and 6, we compare our proposed demodulation criterion using the *net* number of adsorbed molecules with the widely used demodulation criterion using the number of *cumulatively*-adsorbed molecules in [14] and [20]. In these two figures, we set the parameters: $k_1 = 10$ μm/s, $k_{-1} = 5$ s^{-1}, $N_{tx} = 300$, $r_r = 10$ μm, $r_0 = 11$ μm, $D = 8$ μm^2/s,
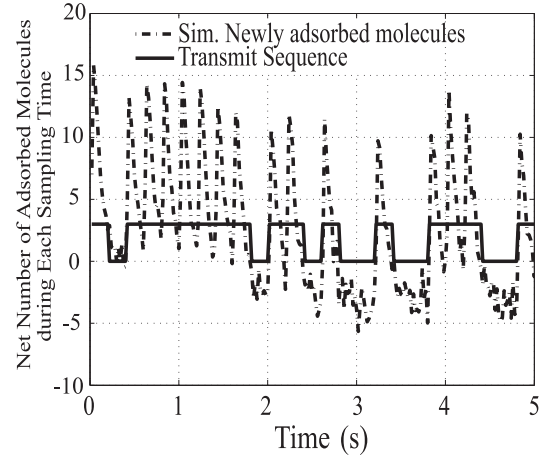
$\Delta t = 10^{-5}$ s, $T_s = 0.02$ s, the bit interval $T_b = 0.2$ s, and the number of bits $N_b = 25$. Fig. 5 plots the number of cumulatively-adsorbed molecules expected at the surface of the A&D receiver in each sampling time due to the transmission of multiple bits, whereas Fig. 6 plots the net number of adsorbed molecules expected at the surface of the A&D receiver at each sampling time due to the transmission of multiple bits. In both figures, the solid lines plot the transmit sequence, where each bit can be bit-0 or bit-1. Note that in both figures, the y-axis values of the transmit signal for bit-0 are zero, and those for bit-1 are scaled in order to clearly show the relationship between the transmit sequence and the number of adsorbed molecules. The dashed lines are plotted by averaging the number of adsorbed molecules over 1000 independent emissions for the same generated transmit sequence in the simulation.

In Fig. 5, it is shown that the number of *cumulatively*-adsorbed molecules expected at the surface of the A&D receiver increases in bit-1 bit intervals, but can decrease in bit-0 bit intervals. This is because the new information molecules injected into the environment due to bit-1 increases the number of cumulatively-adsorbed molecules, whereas, without new molecules due to bit-0, the desorption reaction can eventually decrease the cumulative number of adsorbed molecules. In Fig. 6, we observe a single peak net number of adsorbed molecules for each bit-1 transmitted, similar to the channel response for a single bit-1 transmission in Fig. 1. We also see a noisier signal in each bit-0 interval due to the ISI effect brought by the previous transmit signals.

To motivate our proposed demodulation criterion, we compare the behaviours of the accumulatively and net change of adsorbed molecules at the receiver in Fig. 5 and Fig. 6. We see that the number of cumulatively-adsorbed molecules increases with increasing time, whereas the met number of adsorbed molecules have comparable value (between 10 and 15) for all bit-1 signals. As such, the threshold for demodulating the number of cumulatively-adsorbed molecules should be increased as time increases, while the same threshold can be used to demodulate the net number of adsorbed molecules in different bit intervals. We claim that the received signal should be
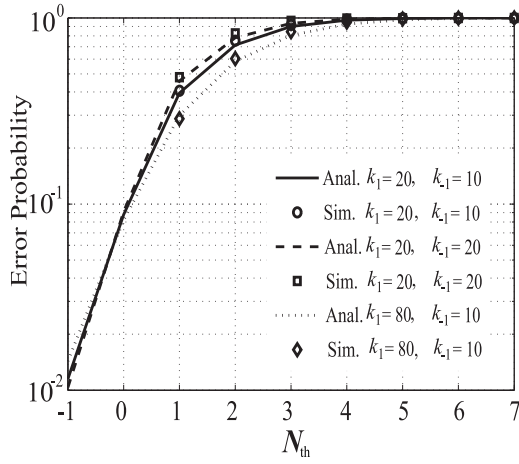
Fig. 7. The error probability for the last transmit bit-1.

Fig. 8. The error probability for the last transmit bit-0.

Fig. 9. The error probability for the last random transmit bit.

demodulated using the net number of adsorbed molecules. Note that the net number of adsorbed molecules refers to the *net* change, since the receiver cannot distinguish between the molecules that just adsorbed and those that were already adsorbed.

D. Error Probability

Figs. 7 and 8 plot the error probability as a function of decision threshold for the third bit in a 3-bit sequence where the last bit is bit-1 and bit-0, respectively. The first 2 bits are "1 1". In these two figures, we set the parameters: $N_{tx} = 50$, $r_r = 15$ μm, $r_0 = 20$ μm, $D = 5$ μm^2/s, $\Delta t = 10^{-6}$ s, $T_s = 0.002$ s, and the bit interval $T_b = 0.2$ s. Note that with lower diffusion coefficient and larger distance between the transmitter and the receiver, a weaker signal is observed. The simulation results are compared with the evaluation of (27) for bit-1 and (30) for bit-0, where the net number of adsorbed molecules expected at the surface of the receiver are approximated by the Skellam distribution. There are negative thresholds with meaningful error probabilities, thus confirming the need for the Skellam distribution. The simulation points are plotted by averaging the total errors over 10^5 independent emissions of transmit sequences with last bit-1 and bit-0. In both figures, we see a close match between the simulation points and the analytical lines.

Fig. 7 plots the error probability of the last transmit bit-1 at the A&D receiver with $N_b = 3$ bits transmitted for various adsorption rate k_1 and desorption rate k_{-1}. We see that the error probability of the last transmit bit-1 increases monotonically with increasing threshold N_{th}. Interestingly, we find that for the same k_{-1}, the error probability improves with increasing k_1. This can be explained by the fact that increasing k_1 increases the amplitude of the net number of adsorbed molecules expected (as shown in Fig. 1), which makes the received signal for bit-1 more distinguishable than that for bit-0. For the same k_1, the error probability degrades with increasing k_{-1}, which is because the received signal for bit-1 is less distinguishable than that for bit-0 with increasing k_{-1}, as shown in Fig. 2.
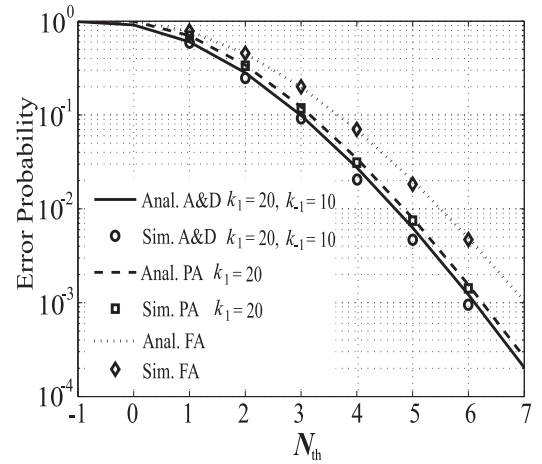
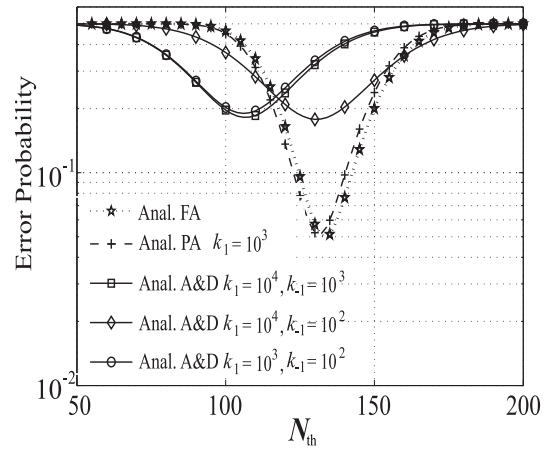Fig. 8 plots the error probability of the last transmit bit-0 for different types of receivers with $N_b = 3$ bits transmitted. The error probability of the full adsorption receiver and the partial adsorption receiver are plotted using (32) and (33). We see that the error probability of the last transmit bit-0 decreases monotonically with increasing the threshold N_{th}. Interestingly, we see that the error probability of the A&D receiver with $k_1 = 20$ μm/s and $k_{-1} = 10$ s^{-1} outperforms that of the partial adsorption receiver with $k_1 = 20$ μm/s and that of the full adsorption receiver, which is due to the higher tail effect from previous bits imposed on the partial adsorption receiver and the full adsorption receiver compared to that imposed on the A&D receiver with $k_{-1} = 10$ s^{-1} as shown in Fig. 3.

Fig. 9 plots the analytical results of the error probability of the last random transmit bit for different types of receivers with various k_1 and k_{-1} using (31), considering that the analytical results have been verified in Figs. 7 and 8. We set the parameters: $N_{tx} = 1000$, $r_r = 5$ μm, $r_0 = 10$ μm, $D = 79.4$ μm^2/s, $T_s = 0.002$ s, $T_b = 0.05$ s, $P_1 = P_0 = 0.5$, and the first 2 bits "1 1". Interestingly, we see that the error probability of the last random bit of the A&D receiver is lower than that of the full adsorption receiver and the partial adsorption receiver for $N_{th} < 110$, and higher than that of the full adsorption

receiver and the partial adsorption receiver for $N_{\text{th}} > 120$. The observations are consistent with what we expected, and can be explained by the advantage due to a lower tail at the A&D receiver than that at the other receivers at *lower detection thresholds*, and the advantage due to a higher peak at the other receivers than that at the A&D receiver at *higher detection thresholds*. We also observe that overall the PA and FA have lower optimal bit error probability. The A&D receiver with $k_1 = 10^4$ and $k_{-1} = 10^3$ achieves comparable bit error probability value as that with $k_1 = 10^3$ and $k_{-1} = 10^2$, which may due to having the same k_1/k_{-1} ratio.

VII. CONCLUSION

In this paper, we modeled the diffusion-based MC system with the A&D receiver. We derived the exact expression for the net number of adsorbed information molecules expected at the surface of the receiver. We also derived the asymptotic expression for the expected number of adsorbed information molecules as the bit interval goes to infinity. We then derived the bit error probability of the A&D receiver. We also presented a simulation algorithm that captures the behavior of each information molecule with the stochastic reversible reaction at the receiver.

Our results showed that the error probability of the A&D receiver can be approximated by the Skellam distribution, and our derived analytical results closely matched our simulation results. We revealed that the error probability of the A&D receiver for the transmit bit-1 improves with increasing adsorption rate and with decreasing desorption rate. More importantly, the error probability of the A&D receiver for the last transmitted bit is worse at higher detection thresholds but better at low detection thresholds than both the full adsorption and partial adsorption receivers. This is because the A&D receiver observes a lower peak number of adsorbed molecules but then a faster decay. Our analytical model and simulation framework provide a foundation for the accurate modeling and analysis of a more complex and realistic receiver in molecular communication.

APPENDIX

PROOF OF THEOREM 1

We first partition the spherically symmetric distribution into two parts using the method applied in [26]

$$r \cdot C(r, t|r_0) = r \cdot g(r, t|r_0) + r \cdot h(r, t|r_0), \quad (50)$$

where

$$g(r, t \to 0|r_0) = \frac{1}{4\pi r_0}\delta(r - r_0), \quad (51)$$

$$h(r, t \to 0|r_0) = 0. \quad (52)$$

Then, by substituting (50) into (3), we have

$$\frac{\partial(r \cdot g(r, t|r_0))}{\partial t} = D\frac{\partial^2(r \cdot g(r, t|r_0))}{\partial r^2}, \quad (53)$$

and

$$\frac{\partial(r \cdot h(r, t|r_0))}{\partial t} = D\frac{\partial^2(r \cdot h(r, t|r_0))}{\partial r^2}. \quad (54)$$

To derive $g(r, t|r_0)$, we perform a Fourier transformation on $rg(r, t|r_0)$ to yield

$$G(k, t|r_0) = \int_{-\infty}^{\infty} rg(r, t|r_0)e^{-ikr}dr, \quad (55)$$

and

$$r \cdot g(r, t|r_0) = \frac{1}{2\pi} \int_{-\infty}^{\infty} G(k, t|r_0)e^{ikr}dk. \quad (56)$$

We then perform the Fourier transformation on (53) to yield

$$\frac{dG(k, t|r_0)}{dt} = -Dk^2 G(k, t|r_0). \quad (57)$$

According to (57) and the uniqueness of the Fourier transform, we derive

$$G(k, t|r_0) = K_g \exp\left\{-Dk^2 t\right\}, \quad (58)$$

where K_g is an undetermined constant.

The Fourier transformation performed on (51) yields

$$G(r, t \to 0|r_0) = \frac{1}{4\pi r_0}e^{-ikr_0}. \quad (59)$$

Combining (58) and (59), we arrive at

$$G(k, t|r_0) = \frac{1}{4\pi r_0}e^{-ikr_0}\exp\left\{-Dk^2 t\right\}. \quad (60)$$

Substituting (60) into (56), we find that

$$r \cdot g(r, t|r_0) = \frac{1}{8\pi r_0\sqrt{\pi Dt}}\exp\left\{-\frac{(r - r_0)^2}{4Dt}\right\}. \quad (61)$$

By performing the Laplace transform on (61), we write

$$\mathcal{L}\{r \cdot g(r, t|r_0)\} = \frac{1}{8\pi r_0\sqrt{Ds}}\exp\left\{-|r - r_0|\sqrt{\frac{s}{D}}\right\}. \quad (62)$$

We then focus on solving the solution $h(k, t|r_0)$ by first performing the Laplace transform on $h(k, t|r_0)$ and (54) as

$$H(r, s|r_0) = \mathcal{L}\{h(r, t|r_0)\} = \int_0^{\infty} h(r, t|r_0)e^{-s\tau}d\tau, \quad (63)$$

and

$$srH(r, s|r_0) = D\frac{\partial^2(rH(r, s|r_0))}{\partial r^2}, \quad (64)$$

respectively.

According to (64), the Laplace transform of the solution with respect to the boundary condition in (64) is

$$rH(r, s|r_0) = f(s)\exp\left\{-\sqrt{\frac{s}{D}}r\right\}, \quad (65)$$

where $f(s)$ needs to satisfy the second initial condition in (4), and the second boundary condition in (5) and (6).

Having the Laplace transform of $\{r \cdot g(r, t|r_0)\}$ and $h(r, t|r_0)$ in (62) and (65), and performing a Laplace transformation on (50), we derive

$$\tilde{r}C(r, s|r_0) = G(r, s|r_0) + rH(r, s|r_0)$$
$$= \frac{1}{8\pi r_0\sqrt{Ds}}\exp\left\{-|r - r_0|\sqrt{\frac{s}{D}}\right\}$$
$$+ f(s)\exp\left\{-\sqrt{\frac{s}{D}}r\right\}, \quad (66)$$

where $\tilde{C}(r, s|r_0) = \int_0^{\infty} C(r, t|r_0)e^{-st}dt$.

We deviate from the method in [26], and perform the Laplace transform on the Robin boundary condition in (7) to solve $f(s)$, which yields

$$\tilde{C}_a(s|r_0) = \frac{k_1 \tilde{C}(r_r, s|r_0)}{s + k_{-1}}, \tag{67}$$

where $\tilde{C}_a(r, s|r_0) = \int_0^\infty C_a(r, t|r_0)e^{-st}dt$.

We then perform the Laplace transform on the second initial condition in (4) and the second boundary condition in (5) as

$$D\frac{\partial\left(\tilde{C}(r, s|r_0)\right)}{\partial r}\bigg|_{r=r_r} = k_1 \tilde{C}(r_r, s|r_0) - k_{-1}\tilde{C}_a(s|r_0). \tag{68}$$

Substituting (67) into (68), we obtain

$$D\frac{\partial\left(\tilde{C}(r, s|r_0)\right)}{\partial r}\bigg|_{r=r_r} = \frac{k_1 s}{s + k_{-1}}\tilde{C}(r_r, s|r_0). \tag{69}$$

To facilitate the analysis, we express the Laplace transform on the second boundary condition as

$$\frac{\partial\left(r \cdot \tilde{C}(r, s|r_0)\right)}{\partial r}\bigg|_{r=r_r} = \left(1 + \frac{r_r k_1 s}{D(s + k_{-1})}\right)\tilde{C}(r, s|r_0). \tag{70}$$

Substituting (66) into (70), we determine $f(s)$ as

$$f(s) = \frac{\left(\sqrt{\frac{s}{D}} - \frac{1}{r_r} - \frac{k_1 s}{D(s+k_{-1})}\right)\exp\left\{-(r_0 - 2r_r)\sqrt{\frac{s}{D}}\right\}}{\left(\sqrt{\frac{s}{D}} + \frac{1}{r_r} + \frac{k_1 s}{D(s+k_{-1})}\right) 8\pi r_0 \sqrt{Ds}}. \tag{71}$$

Having (66) and (71), and performing the Laplace transform of the concentration distribution, we derive

$$r\tilde{C}(r, s|r_0) = \frac{1}{8\pi r_0 \sqrt{Ds}}\exp\left\{-|r - r_0|\sqrt{\frac{s}{D}}\right\}$$
$$+ \frac{1}{8\pi r_0 \sqrt{Ds}}\exp\left\{-(r + r_0 - 2r_r)\sqrt{\frac{s}{D}}\right\}$$
$$- \underbrace{\frac{2\left(\frac{1}{r_r} + \frac{k_1 s}{D(s+k_{-1})}\right)\exp\left\{-(r + r_0 - 2r_r)\sqrt{\frac{s}{D}}\right\}}{8\pi r_0 \sqrt{Ds}\left(\frac{1}{r_r} + \frac{k_1 s}{D(s+k_{-1})} + \sqrt{\frac{s}{D}}\right)}}_{Z(s)}. \tag{72}$$

Applying the inverse Laplace transform leads to

$$rC(r, s|r_0) = \frac{1}{8\pi r_0 \sqrt{\pi Dt}}\exp\left\{-\frac{(r - r_0)^2}{4Dt}\right\}$$
$$+ \frac{1}{8\pi r_0 \sqrt{\pi Dt}}\exp\left\{-\frac{(r + r_0 - 2r_r)^2}{4Dt}\right\}$$
$$- \mathcal{L}^{-1}\{Z(s)\}. \tag{73}$$

Due to the complexity of $Z(s)$, we can not derive the closed-form expression for its inverse Laplace transform $f_z(t) = \mathcal{L}^{-1}\{Z(s)\}$. We employ the Gil-Pelaez theorem [49] for the

characteristic function to derive the cumulative distribution function (CDF) $F_z(t)$ as

$$F_z(t) = \frac{1}{2} - \frac{1}{\pi}\int_0^\infty \frac{\mathrm{Im}\left[e^{-jwt}\varphi_Z(w)\right]}{w}dw,$$
$$= \frac{1}{2} - \frac{1}{\pi}\int_0^\infty \frac{e^{-jwt}\varphi_Z^*(w) - e^{jwt}\varphi_Z(w)}{2jw}dw, \tag{74}$$

where $\varphi_Z(w)$ is given in (9).

Taking the derivative of $F_z(t)$, we derive the inverse Laplace transform of $Z(s)$ as

$$f_z(t) = \frac{1}{2\pi}\int_0^\infty \left(e^{-jwt}\varphi_Z^*(w) + e^{jwt}\varphi_Z(w)\right)dw. \tag{75}$$

Combining (9) and (73), we finally derive the expected time-varying spatial distribution in (8).

REFERENCES

[1] Y. Deng, A. Noel, M. Elkashlan, A. Nallanathan, and K. C. Cheung, "Molecular communication with a reversible adsorption receiver," in *Proc. IEEE ICC*, Jun. 2016.

[2] T. Nakano, A. W. Eckford, and T. Haraguchi, *Molecular Communication*, 1st ed. Cambridge, U.K.: Cambridge Univ. Press, 2013.

[3] N. Farsad, H. B. Yilmaz, A. Eckford, C.-B. Chae, and W. Guo, "A comprehensive survey of recent advancements in molecular communication," *IEEE Commun. Surveys Tuts.*, to be published.

[4] T. Nakano, M. J. Moore, F. Wei, A. V. Vasilakos, and J. Shuai, "Molecular communication and networking: Opportunities and challenges," *IEEE Trans. Nanobiosci.*, vol. 11, no. 2, pp. 135–148, Jun. 2012.

[5] M. Moore *et al.*, "A design of a molecular communication system for nanomachines using molecular motors," in *Proc. 4th Annu. IEEE Int. Conf. PerCom Workshops*, Pisa, Italy, Mar. 2006, pp. 554–559.

[6] H. C. Berg, *Random Walks in Biology*. Princeton, NJ, USA: Princeton Univ. Press, 1993.

[7] T. Nakano *et al.*, "Molecular communication for nanomachines using intercellular calcium signaling," in *Proc. IEEE NANO*, vol. 2. Nagoya, Japan, 2005, pp. 478–481.

[8] W. H. Bossert and E. O. Wilson, "The analysis of olfactory communication among animals," *J. Theor. Biol.*, vol. 5, no. 3, pp. 443–469, Nov. 1963.

[9] A. W. Eckford, "Nanoscale communication with Brownian motion," in *Proc. Conf. Inf. Sci. Syst.*, Baltimore, MD, USA, 2007, pp. 160–165.

[10] S. Kadloor, R. S. Adve, and A. W. Eckford, "Molecular communication using Brownian motion with drift," *IEEE Trans. Nanobiosci.*, vol. 11, no. 2, pp. 89–99, Jun. 2012.

[11] S. Kadloor and R. Adve, "A framework to study the molecular communication system," in *Proc. ICCCN*, San Francisco, CA, USA, Aug. 2009, pp. 1–6.

[12] K. V. Srinivas, A. W. Eckford, and R. S. Adve, "Molecular communication in fluid media: The additive inverse Gaussian noise channel," *IEEE Trans. Inf. Theory*, vol. 58, no. 7, pp. 4678–4692, Jul. 2012.

[13] M. Egan, Y. Deng, M. Elkashlan, and T. Q. Duong, "Variance-constrained capacity of the molecular timing channel with synchronization error," in *Proc. GLOBECOM*, Austin, TX, USA, Dec. 2014, pp. 1473–1478.

[14] A. Noel, K. C. Cheung, and R. Schober, "Improving receiver performance of diffusive molecular communication with enzymes," *IEEE Trans. Nanobiosci.*, vol. 13, no. 1, pp. 31–43, Mar. 2014.

[15] H. B. Yilmaz, A. C. Heren, T. Tugcu, and C.-B. Chae, "Three-dimensional channel characteristics for molecular communications with an absorbing receiver," *IEEE Commun. Lett.*, vol. 18, no. 6, pp. 929–932, Jun. 2014.

[16] H. B. Yilmaz and C.-B. Chae, "Simulation study of molecular communication systems with an absorbing receiver: Modulation and ISI mitigation techniques," *Simulat. Model. Pract. Theory*, vol. 49, pp. 136–150, Dec. 2014.

[17] C. T. Chou, "A Markovian approach to the optimal demodulation of diffusion-based molecular communication networks," *IEEE Trans. Commun.*, vol. 63, no. 10, pp. 3728–3743, Oct. 2015.

[18] B. Tepekule, A. E. Pusane, H. B. Yilmaz, C.-B. Chae, and T. Tugcu, "ISI mitigation techniques in molecular communication," *IEEE Trans. Mol. Biol. Multi Scale Commun.*, vol. 1, no. 2, pp. 202–216, Jun. 2015.

[19] P. Cuatrecasas, "Membrane receptors," *Annu. Rev. Biochem.*, vol. 43, no. 1, pp. 169–214, 1974.

[20] A. Noel, K. C. Cheung, and R. Schober, "Optimal receiver design for diffusive molecular communication with flow and additive noise," *IEEE Trans. Nanobiosci.*, vol. 13, no. 3, pp. 350–362, Sep. 2014.

[21] Y. Deng, A. Noel, W. Guo, A. Nallanathan, and M. Elkashlan, "Stochastic geometry model for large-scale molecular communication systems," in *Proc. IEEE GLOBECOM*, Washington, DC, USA, Dec. 2016.

[22] J.-P. Rospars, V. Krivan, and P. Lansky, "Perireceptor and receptor events in olfaction. Comparison of concentration and flux detectors: A modeling study," *Chem. Senses*, vol. 25, no. 3, pp. 293–311, Jun. 2000.

[23] S. F. Bush, *Nanoscale Communication Networks*. Boston, MA, USA: Artech House, 2010.

[24] T. Suda, M. Moore, T. Nakano, R. Egashira, and A. Enomoto, "Exploratory research on molecular communication between nanomachines," in *Proc. Genet. Evol. Comput. Conf.*, Washington, DC, USA, 2005.

[25] C. T. Chou, "Extended master equation models for molecular communication networks," *IEEE Trans. Nanobiosci.*, vol. 12, no. 2, pp. 79–92, Jun. 2013.

[26] K. Schulten and I. Kosztin, "Lectures in theoretical biophysics," Univ. Illinois, Champaign, IL, USA, vol. 117, 2000.

[27] J. Feder and I. Giaever, "Adsorption of ferritin," *J. Colloid Interface Sci.*, vol. 78, no. 1, pp. 144–154, Nov. 1980.

[28] J. J. Ramsden, "Concentration scaling of protein deposition kinetics," *Phys. Rev. Lett.*, vol. 71, no. 2, pp. 295–298, Jul. 1993.

[29] F. Fang, J. Satulovsky, and I. Szleifer, "Kinetics of protein adsorption and desorption on surfaces with grafted polymers," *Biophys. J.*, vol. 89, no. 3, pp. 1516–1533, 2005.

[30] I. F. Akyildiz, M. Pierobon, S. Balasubramaniam, and Y. Koucheryavy, "The Internet of bio-nano things," *IEEE Commun. Mag.*, vol. 53, no. 3, pp. 32–40, Mar. 2015.

[31] S. S. Andrews, "Accurate particle-based simulation of adsorption, desorption, and partial transmission," *Phys. Biol.*, vol. 6, no. 4, Nov. 2009, Art. no. 046015.

[32] S. S. Andrews, N. J. Addy, R. Brent, and A. P. Arkin, "Detailed simulations of cell biology with Smoldyn 2.1," *PLoS Comput. Biol.*, vol. 6, no. 3, Mar. 2010, Art. no. e1000705.

[33] I. Llatser, I. Pascual, N. Garralda, A. Cabellos-Aparicio, and E. Alarcón, "N3sim: A simulation framework for diffusion-based molecular communication," 2011.

[34] W. Scheider, "Two-body diffusion problem and applications to reaction kinetics," *J. Phys. Chem.*, vol. 76, no. 3, pp. 349–361, Feb. 1972.

[35] C. Fan, K. W. Plaxco, and A. J. Heeger, "Biosensors based on binding-modulated donor–acceptor distances," *Trends Biotechnol.*, vol. 23, no. 4, pp. 186–192, Apr. 2005.

[36] P. C. Nelson, *Biological Physics: Energy, Information, Life*, 1st ed. New York, NY, USA: W.H. Freeman, 2008.

[37] T. Chou and M. R. D'Orsogna, "Multistage adsorption of diffusing macromolecules and viruses," *J. Chem. Phys.*, vol. 127, no. 10, 2007, Art. no. 105101.

[38] J. Crank, *The Mathematics of Diffusion*, 2nd ed. Oxford, U.K.: Oxford Univ. Press, 1980.

[39] K. Gustafson and T. Abe, "The third boundary condition—Was it Robin's?" *Math. Intell.*, vol. 20, no. 1, pp. 63–71, 1998. [Online]. Available: http://dx.doi.org/10.1007/BF03024402

[40] M. S. Kuran, H. B. Yilmaz, T. Tugcu, and I. F. Akyildiz, "Modulation techniques for communication via diffusion in nanonetworks," in *Proc. IEEE ICC*, Kyoto, Japan, Jun. 2011, pp. 1–5.

[41] N.-R. Kim and C.-B. Chae, "Novel modulation techniques using isomers as messenger molecules for nano communication networks via diffusion," *IEEE J. Sel. Areas Commun.*, vol. 31, no. 12, pp. 847–856, Dec. 2013.

[42] H. B. Yilmaz and C.-B. Chae, "Arrival modelling for molecular communication via diffusion," *Electron. Lett.*, vol. 50, no. 23, pp. 1667–1669, Nov. 2014.

[43] A. C. Heren, H. B. Yilmaz, C.-B. Chae, and T. Tugcu, "Effect of degradation in molecular communication: Impairment or enhancement?" *IEEE Trans. Mol. Biol. Multi Scale Commun.*, vol. 1, no. 2, pp. 217–229, Jun. 2015.

[44] M. Ş. Kuran, H. B. Yilmaz, T. Tugcu, and B. Özerman, "Energy model for communication via diffusion in nanonetworks," *Nano Commun. Netw.*, vol. 1, no. 2, pp. 86–95, 2010.

[45] M. Natrella, *NIST/SEMATECH e-Handbook of Statistical Methods*. Gaithersburg, MD, USA: Nat. Inst. Stand. Technol., 2010.

[46] D. Karlis and I. Ntzoufras, "Analysis of sports data by using bivariate poisson models," *J. Roy. Stat. Soc. D*, vol. 52, no. 3, pp. 381–393, 2003.

[47] S. S. Andrews and D. Bray, "Stochastic simulation of chemical reactions with spatial resolution and single molecule detail," *Phys. Biol.*, vol. 1, nos. 3–4, pp. 137–151, 2004.

[48] R. Erban and S. J. Chapman, "Reactive boundary conditions for stochastic simulations of reaction–diffusion processes," *Phys. Biol.*, vol. 4, no. 1, pp. 16–28, Feb. 2007.

[49] J. G. Wendel, "The non-absolute convergence of Gil-Pelaez' inversion integral," *Ann. Math. Stat.*, vol. 32, no. 1, pp. 338–339, Mar. 1961.

Yansha Deng (S'13–M'16) received the Ph.D. degree in electrical engineering from the Queen Mary University of London, U.K., in 2015. She is currently the Post-Doctoral Research Fellow with the Department of Informatics, King's College London, U.K. Her research interests include massive MIMO, HetNets, molecular communication, cognitive radio, cooperative networks, and physical layer security. She has served as a TPC member for many IEEE conferences, such as the IEEE GLOBECOM and ICC. She was a recipient of the Best Paper Award at ICC 2016.

Adam Noel (S'09–M'16) received the B.Eng. degree in electrical engineering from Memorial University, St. John's, Canada, in 2009, the M.A.Sc. degree in electrical engineering and the Ph.D. degree in electrical and computer engineering from the University of British Columbia, Vancouver, Canada, in 2011 and 2015, respectively. In 2013, he was a Visiting Scientist with the Institute for Digital Communication, Friedrich-Alexander-University, Erlangen, Germany. He is currently a Post-Doctoral Fellow with the University of Ottawa, Ottawa, Canada. His current research interests include channel modeling, system design, and simulation methods for molecular communication networks.

Maged Elkashlan (M'06) received the Ph.D. degree in electrical engineering from the University of British Columbia, in 2006. From 2007 to 2011, he was with the Wireless and Networking Technologies Laboratory, Commonwealth Scientific and Industrial Research Organization, Australia. During this time, he held an adjunct appointment with the University of Technology Sydney, Australia. In 2011, he joined the School of Electronic Engineering and Computer Science, Queen Mary University of London, U.K., as an Assistant Professor. He also holds visiting faculty appointments with the University of New South Wales, Australia, and the Beijing University of Posts and Telecommunications, China. His research interests include massive MIMO, millimeter wave communications, and heterogeneous networks.

He currently serves as an Editor for the IEEE TRANSACTIONS ON WIRELESS COMMUNICATIONS, the IEEE TRANSACTIONS ON VEHICULAR TECHNOLOGY, and the IEEE COMMUNICATIONS LETTERS. He was a recipient of the Best Paper Award at the IEEE International Conference on Communications in 2016 and 2014, the International Conference on Communications and Networking in China in 2014, and the IEEE Vehicular Technology Conference (VTC-Spring) in 2013.

Arumugam Nallanathan (S'97–M'00–SM'05) is a Professor of Wireless Communications with the Department of Informatics, King's College London (University of London). He served as the Head of Graduate Studies with the School of Natural and Mathematical Sciences, King's College London, from 2011 to 2012. He was an Assistant Professor with the Department of Electrical and Computer Engineering, National University of Singapore, from 2000 to 2007. He published nearly 300 technical papers in scientific journals and international conferences. His research interests include 5G wireless networks, molecular communications, energy harvesting, and cognitive radio networks. He is an IEEE Distinguished Lecturer.

He was a recipient of the IEEE Communications Society SPCE Outstanding Service Award 2012 and the IEEE Communications Society RCC Outstanding Service Award 2014. He is an Editor for the IEEE TRANSACTIONS ON COMMUNICATIONS and the IEEE TRANSACTIONS ON VEHICULAR TECHNOLOGY. He was an Editor of the IEEE TRANSACTIONS ON WIRELESS COMMUNICATIONS from 2006 to 2011, the IEEE WIRELESS COMMUNICATIONS LETTERS and the IEEE SIGNAL PROCESSING LETTERS. He served as the Chair for the Signal Processing and Communication Electronics Technical Committee of the IEEE Communications Society, the Technical Program Co-Chair (MAC track) for the IEEE WCNC 2014, the Co-Chair for the IEEE GLOBECOM 2013 (Communications Theory Symposium), the IEEE ICC 2012 (Signal Processing for Communications Symposium), the IEEE GLOBECOM 2011 (Signal Processing for Communications Symposium), the IEEE ICC 2009 (Wireless Communications Symposium), the IEEE GLOBECOM 2008 (Signal Processing for Communications Symposium), the Technical Program Co-Chair for the IEEE International Conference on UWB 2011 (IEEE ICUWB 2011), and the General Track Chair for IEEE VTC 2008. He was a co-recipient of the Best Paper Award presented at the IEEE International Conference on Communications 2016 and the IEEE International Conference on Ultra-Wideband 2007.

Karen C. Cheung received the B.S. and Ph.D. degrees in bioengineering from the University of California, Berkeley, CA, USA, in 1998 and 2002, respectively. From 2002 to 2005, she was a Post-Doctoral Researcher with the École Polytechnique Fédérale de Lausanne, Lausanne, Switzerland. She is currently with the University of British Columbia, Vancouver, Canada. Her research interests include lab-on-a-chip systems for cell-based drug screening, inkjet printing for tissue engineering, and implantable neural interfaces.